ACS APPLIED MATERIALS & INTERFACES

Research Article

www.acsami.org

A New Approach to Reducing the Flammability of Layered Double Hydroxide (LDH)-Based Polymer Composites: Preparation and Characterization of Dye Structure-Intercalated LDH and Its Effect on the Flammability of Polypropylene-Grafted Maleic Anhydride/d-LDH Composites

Nian-Jun Kang,[†] De-Yi Wang,*[,†] Burak Kutlu,[‡,§] Peng-Cheng Zhao,[§] Andreas Leuteritz,[‡] Udo Wagenknecht,[‡] and Gert Heinrich[‡,§]

[†]Madrid Institute for Advanced Studies of Materials (IMDEA Materials), C/Eric Kandel, 2, 28906 Getafe, Madrid, Spain

[‡]Leibniz-Institut für Polymerforschung Dresden e.V., Hohe Strasse 6, D-01069 Dresden, Germany

[§]Technische Universität Dresden, Institut für Werkstoffwissenschaft, D-01069 Dresden, Germany

ABSTRACT: Dye structure-intercalated layered double hydroxide (d-LDH) was synthesized using a one-step method, and its intercalated behaviors have been characterized by Fourier transform infrared spectroscopy (FTIR), wide angle X-ray scattering (WAXS), scanning electron microscopy, thermogravimetric analysis (TGA), etc. As a novel functional potential fire-retarding nanofiller, it was used to prepare a polypropylene-grafted maleic anhydride (PP-g-MA)/d-LDH composite by refluxing the mixture of d-LDH and PP-g-MA in xylene, aiming to investigate its effect on the flammability of the PP-g-MA composite. The morphological properties, thermal stability, and flame retardant properties of the PP-g-MA/d-LDH composite were determined by FTIR, WAXS, transmission electron microscopy, TGA, and microscale combustion calorimetry. Compared with NO_3-LDH (unmodified LDH) and LDH intercalated by sodium dodecylbenzenesulfonate (conventional organo-modified LDH), d-LDH can significantly decrease the heat release rate and the total heat release of the PP-g-MA composite, offering a new approach to imparting low flammability to LDH-based polymer composites.

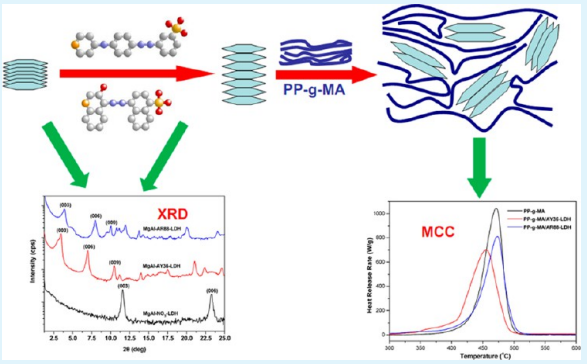

KEYWORDS: *layered double hydroxide (LDH), flammability, polymer composites, dye structure, polypropylene-grafted maleic anhydride, heat release rate*

1. INTRODUCTION

Layered double hydroxides (LDHs), also known as anionic clays, make up a class of host−guest material that has positively charged brucite-like sheets, between which intercalated anions and, in general, some water molecules are located.[1] The charge on the octahedral sheets is created by substituting some divalent cations with their suitable trivalent alternatives. The charge-balancing anions, such as inorganic acids,[2] amino acids,[3−5] and anionic polymer,[6,7] are encapsulated in the interlayer space and easily exchanged with various anions. LDHs can be represented by the chemical formula $[M^{2+}_{1-x}M^{3+}_{x}(OH)_2]^{x+}A^{n-}_{x/n}\cdot yH_2O$, where M^{2+}, M^{3+}, and A^{n-} are divalent metal cations, trivalent metal cations, and interlayer anions, respectively.[8] The species of M^{2+}, M^{3+}, and A^{n-} together with the value of x can be varied to give rise to a large of class of isostructural LDHs.

LDHs have been widely used as nanofillers in polymer composites because of their highly tunable properties.[9−12] Considering the efforts to enlarge the interlayer distance and exfoliate LDH layers, the use of LDH as nanofillers indicates an emerging domain of application, in which LDH is superior to natural clay particles because of its versatility in compositions, tunable charge density, and multiple interactions with the matrix.[13] Basically, natural clay, such as montmorillonite or sepiolite, has a relatively high thermal stability and can be used as an effective flame retardant synergist for polymeric materials as combined with flame retardants.[14,15] However, natural clay is less likely to become an excellent flame retardant because of its intrinsic structures. In comparison, LDH can be used as a flame retardant because of its endothermic decomposition upon exposure to high temperatures.[16−18] To be used as nanofiller for polymers, it is necessary to modify the pristine LDH to enlarge the interlayer distance, to alter the surface properties, and to facilitate dispersion in the polymers.[19−22] In fact, a wide variety of anionic surfactants, such as fatty acid salts,[23] sulfonates,[24,25] and phosphates,[26,27] can modify LDH. Among

Received: May 29, 2013
Accepted: August 8, 2013
Published: August 8, 2013

them, sodium dodecylbenzenesulfonate (SDBS) is one of the most widely used.[28−30] It has been estimated that the SDBS-intercalated LDH contains ∼46 wt % metal hydroxide, and the interlayer distance increases from 0.76 nm (pristine LDH) to 2.95 nm.[29] However, SDBS is a flammable surfactant like most modifiers for LDH. Thus, it is risky to decrease the flame retardancy of modified LDH and/or polymer/LDH composites by using SDBS for LDH's modification. In comparison to the structure of SDBS, most of the acid dyes contain nonfused aromatic, naphthalene, or anthracene rings,[31,32] possessing many rigid structures that may lead to the formation of rich-char residues and less volatile fuels during combustion or decomposition.

In this work, two kinds of anionic dyes (as shown in Figure 1) were used to modify LDH. Dye structure-intercalated LDHs

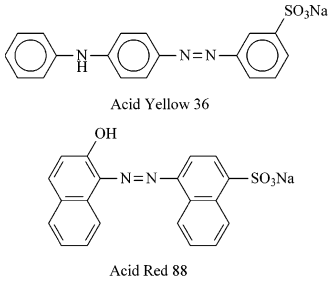

Figure 1. Structures of acid yellow 36 (AY36) and acid red 88 (AR88).

(d-LDHs) were synthesized using a single-step method and characterized by Fourier transform infrared spectroscopy (FTIR), scanning electron microscopy (SEM), wide angle X-ray scattering (WAXS), and thermogravimetric analysis (TGA). Afterwards, d-LDHs were used as flame retardant nanofiller in polypropylene-grafted maleic anhydride (PP-g-MA) to prepare corresponding polymer composites by refluxing the mixture of LDHs and PP-g-MA in xylene. The morphological properties, thermal stability, and flame retardant properties of composites were studied systemically. In comparison, the corresponding polymer composites based on LDH-NO_3 (unmodified LDH) and LDH-SDBS were investigated in parallel.

2. EXPERIMENTAL SECTION

2.1. Materials. Metal nitrate salts [$Mg(NO_3)_2{\cdot}6H_2O$ and $Al(NO_3)_3{\cdot}9H_2O$] were obtained from ABCR Chemical Co. and used without further purification. Sodium hydroxide, SDBS, acid yellow 36 (dye content of 70%, AY36), and acid red 88 (dye content of 75%, AR88) were obtained from Sigma-Aldrich Chemical Co. and used without further purification. PP-g-MA having a degree of grafting of 0.5 wt % MA was used as matrix of polymer/LDH composites.

2.2. Synthesis of Dye Structure-Intercalated LDHs via One-Step Method. Synthesis of dye structure-intercalated LDHs was conducted via a procedure similar to that described in our earlier report.[29] In detail, an aqueous solution containing 0.02 mol (5.13 g) of $Mg(NO_3)_2{\cdot}6H_2O$ and 0.01 mol (3.75 g) of $Al(NO_3)_3{\cdot}9H_2O$ in 100 mL of deionized water was slowly added to a solution containing 0.012 mol (6.44 g) of AY36 or 0.012 mol (6.41 g) of AR88 in 100 mL of deionized water at room temperature. In the synthesis, the pH value was kept at 10 ± 0.2 by adding a 1 mol/L NaOH aqueous solution. Then, the resulting slurry was continuously stirred for 30 min; afterward, it was allowed to age at 75 °C for 18 h. Finally, the resulting product was filtered and washed thoroughly with deionized water until the pH reached 7. The sample was then dried in an oven at 80 °C until a constant weight was achieved. In addition, unmodified LDH and SDBS-intercalated LDH were synthesized via the same method.

2.3. Preparation of PP-g-MA/LDH Composites. Dye structure-intercalated LDH was then used as flame retardant nanofiller for PP-g-MA to prepare PP-g-MA/d-LDH composites. Typical PP-g-MA/LDH composites were prepared by refluxing the mixture with the desired amount of d-LDH (5 wt % in this work) and PP-g-MA in xylene for 24 h. The solution was then poured into 100 mL of ethanol. The precipitate was filtered and dried under vacuum at 80 °C for 24 h. In comparison, PP-g-MA/unmodified LDH and PP-g-MA/SDBS-LDH composites were also prepared by the same method described above.

2.4. Characterization. Fourier transform infrared spectra of the LDH samples were obtained using a BRUKER VERTEX 80V spectrometer over a wavenumber range of 400−4000 cm^{-1}. The powdered samples were mixed with KBr and pressed in the form of pellets for the measurement of FTIR analysis.

Wide angle X-ray scattering (WAXS) was performed using an XRD 3003 θ/θ two-circle diffractometer (GE Inspection Technologies/Seifert-FPM, Freiberg, Germany) with Cu Kα radiation (λ = 0.154 nm) in the range of 2θ = 0.5−25° using a step length of 0.05°.

Thermogravimetric analysis was conducted using a TA Instruments TGA Q 5000 instrument in the range between room temperature and 800 °C at a heating rate of 10 K/min in a nitrogen atmosphere. Interactions between the compounds can be illuminated by comparing the experimental results with the calculated results (W_{calc}) as a linear combination of the TG results of the mixture ingredients weighted by their contents.

$$W_{calc}(T) = \sum_{i=1}^{n} x_i W_i(T)$$

where x_i is content of compound i and W_i is the TG result of the compound i.

Elemental analysis was performed using a CHNS analyzer (varioMICRO version 1.5.7), configured to detect carbon, hydrogen, nitrogen, and sulfur. The linear calibration method was selected using three calibration standards for accurate analysis: cystine, sulfanilamide, and BBOT. Approximately 3 mg of sample (including standards) with 5 mg of vanadium pentoxide (V_2O_5) was sealed in tin capsules (8 mm × 5 mm) excluding air, and the samples were analyzed in triplicate. V_2O_5 was added to improve sulfur quantification.

Scanning electron microscopy (SEM) (model LEO 435 VP microscope, Carl Zeiss SMT) was used to study the morphological features of the powdered samples. The samples were placed on a sample holder using conducting carbon cement and then coated with a thin layer of platinum (thickness of 15 nm) using a sputter coater (BAL-TEC SCD 500).

Morphological analysis was conducted using transmission electron microscopy (TEM) with an LEO 912 microscope. The conditions used during analysis were room temperature, an acceleration voltage of 120 kV, and bright field illumination. The ultrathin sections of the samples were prepared by ultramicrotomy at −120 °C with a thickness of 80 nm.

A microscale combustion calorimeter (MCC-1, FTT) is a convenient technique developed in recent years for the investigation of the flammability of polymers. In this system, ∼5 mg samples are heated to 700 °C at a heating rate of 1 K/s under nitrogen. Then, the volatile, anaerobic thermal degradation products are mixed with a 20 cm^3/min gas stream containing 20% oxygen and 80% nitrogen prior to being added to a 900 °C combustion furnace. The parameters measured from this test are the heat release rate (HRR) in watts per gram (calculated from the oxygen depletion measurements), the heat release capacity (HRC) in joules per gram per kelvin (obtained by dividing the sum of the peak HRR by the heating rate in kelvin per second), and the total heat release (THR) in kilojoules per gram (given by integrating the HRR curve). Each composite is measured three times, and the results are averaged.

3. RESULTS AND DISCUSSION

3.1. Characterization of Dye Structure-Intercalated LDH (MgAl-AR88/AY36-LDH). *3.1.1. Fourier Transform*

Infrared Spectra. The FTIR spectra of LDH materials provide important information about the interlayer anions and hence are very useful for confirming the structure of these materials. The FTIR spectra of various reactants and products are shown in Figure 2. The broad band in the range of 3000−3700 cm^{-1}

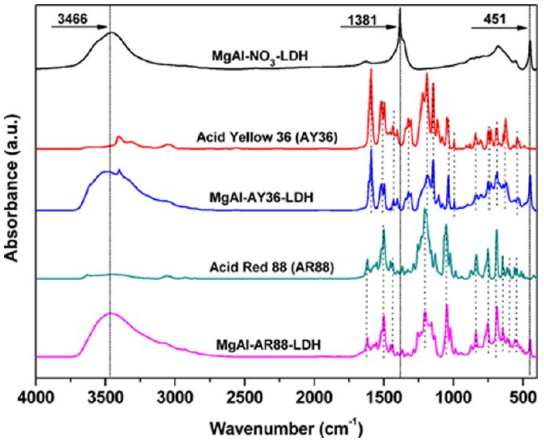

Figure 2. FTIR spectra of MgAl-NO_3-LDH, AY36, MgAl-AY36-LDH, AR88, and MgAl-AR88-LDH samples.

originates from the O−H stretching of the metal hydroxide layer and interlayer water molecules. The banding vibration of the interlayer H_2O is also reflected in the broad bands around 1624 cm^{-1}. In the spectrum of MgAl-NO_3-LDH, the characteristic band for interlayer nitrate (NO_3^-) was clearly observed (1381 cm^{-1}), which disappeared in the cases of MgAl-AY36-LDH and MgAl-AR88-LDH, indicating that the nitrate is almost completely exchanged with dye anion. The bands characteristic of the metal−oxygen bond stretching appear around 451 cm^{-1}. The main differences in the FTIR spectra between MgAl-NO_3-LDH and dye structure-intercalated modified LDHs appeared to be due to the presence of dye ion in the latter. It can be seen that all characteristic bands of AY36 and AR88 were also observed in the spectra of MgAl-AY36-LDH and MgAl-AR88-LDH, respectively. The results indicate the presence of dye molecules in all the modified LDHs and were consistent with the following WAXS results.

3.1.2. Wide Angle X-ray Scattering (WAXS). The WAXS patterns for MgAl-NO_3-LDH and dye-intercalated LDHs are shown in Figure 3. In each case, the patterns exhibit the

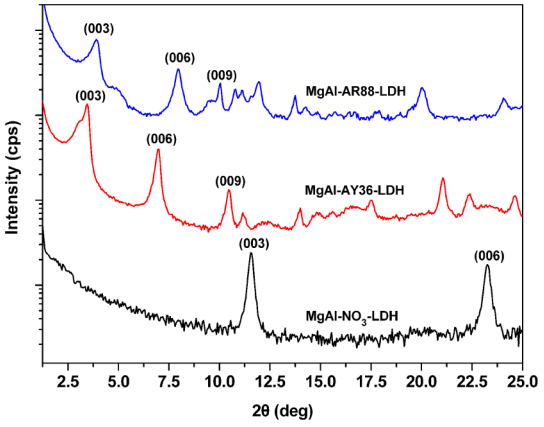

Figure 3. WAXS patterns of MgAl-NO_3-LDH, MgAl-AY36-LDH, and MgAl-AR88-LDH.

characteristic reflections of LDH materials with a series of (003) peaks appearing at low angles, corresponding to the basal spacing and higher-order reflections. In MgAl-NO_3-LDH, the first basal reflection (003) at 2θ = 11.6° corresponds to an interlayer distance of 0.75 nm. In MgAl-AY36-LDH and MgAl-AR88-LDH, the positions of (003) shift to 2θ = 3.45° and 3.90°, indicating interlayer distances of 2.56 and 2.26 nm (calculated by the Bragg equation), respectively. The obtained results show the dye-intercalated LDHs possess a >3-fold increase in interlayer distance compared to that of MgAl-NO_3-LDH.

The crystallographic structures of the dye-intercalated LDHs are schematically shown in Figure 4. According to a previous

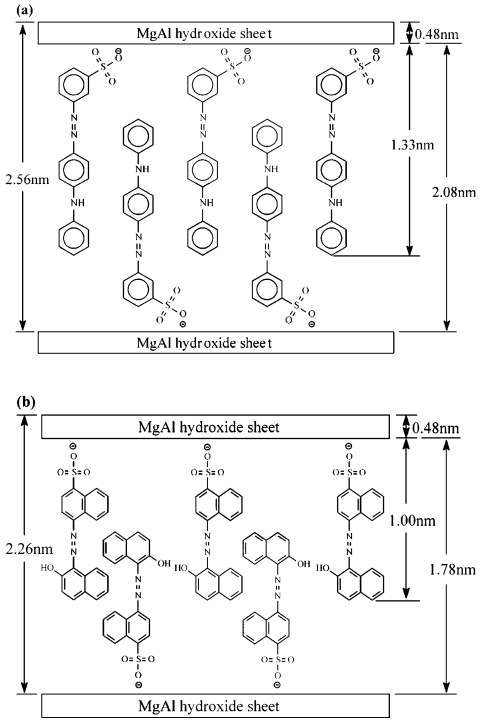

Figure 4. Crystallographic structure of dye-intercalated LDH: (a) MgAl-AY36-LDH and (b) MgAl-AR88-LDH.

report,[6] the thickness of MgAl hydroxide sheets is 0.48 nm, so the gallery height between the MgAl hydroxide sheets for AY36- and AR88-intercalated LDH can be calculated as 2.08 and 1.78 nm, respectively. This means the structures of AY36 and AR88 anions are interdigitated in the interlayer space because the approximate lengths of molecules AY36 and AR88 are 1.36 and 1.00 nm, respectively, calculated by ChemOffice (as shown in Figure 5)

3.1.3. Scanning Electron Microscopy (SEM). Figure 6 shows SEM images of MgAl-NO_3-LDH and dye-intercalated LDHs samples. As one can see, MgAl-NO_3-LDH has a platelike geometry of its primary particles with a microscopically smooth surface. In general, though no particular particle shape can be observed, the existence of sharp edges in most of the particles may be an indication of the incomplete crystal growth process. This process requires sufficient and suitable postsynthesis treatment of LDH particles resulting in perfect hexagonal geometry of the LDH particles. On the other hand, the morphology of the dye-intercalated LDHs is somewhat different. Because of the expansion of the basal spacing after

dx.doi.org/10.1021/am4020555 | ACS Appl. Mater. Interfaces 2013, 5, 8991−8997

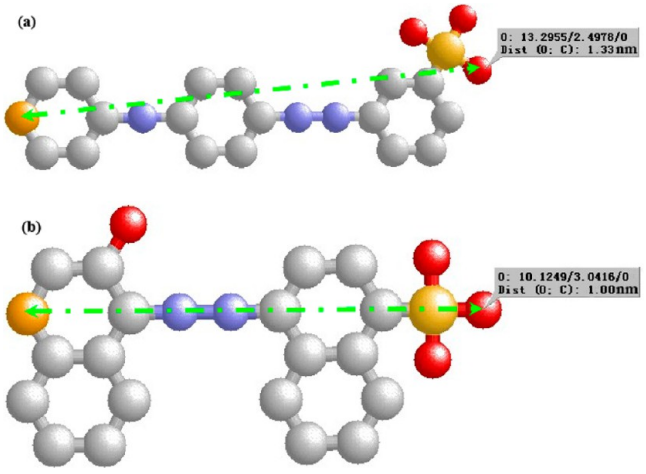

Figure 5. Molecule structure and size of (a) AY36 and (b) AR88.

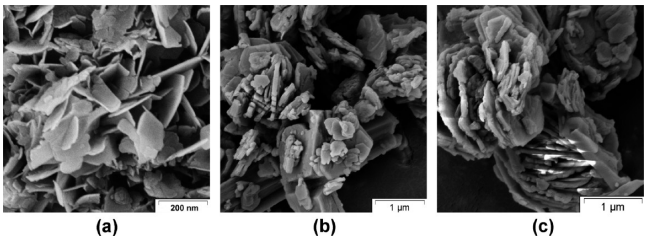

Figure 6. SEM of (a) MgAl-NO_3-LDH, (b) MgAl-AY36-LDH, and (c) MgAl-AR88-LDH.

the intercalation of dye anions, the surface becomes much rougher and the LDH layers become thicker.

3.1.4. Elemental Analysis (EA) and Thermogravimetric Analysis (TGA). Elemental analysis of dye-intercalated LDHs along with their thermograms is shown in Figure 7. The d-

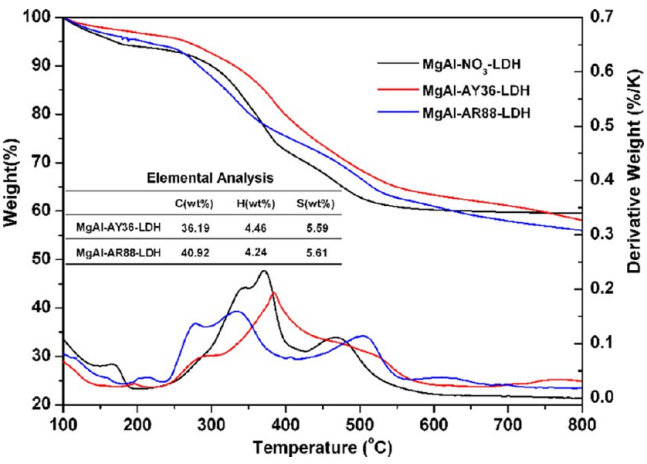

Figure 7. TGA profiles of MgAl-NO_3-LDH, MgAl-AY36-LDH, and MgAl-AR88-LDH.

LDHs could be represented by the chemical formula $Mg_2Al\cdot(OH)_6\cdot(\text{dye anion})_x\cdot(NO_3)_{1-x}\cdot 0.4H_2O$, where the dye anion is AY36 or AR88 and x is the degree of intercalation of the dye anion. On the basis of elemental analysis data of sulfur [S(wt %)], the degree of intercalation of AY36 or AR88 (x) can be calculated from the equation

$$S(\text{wt}\,\%) = \frac{32x}{246.2 + x(M_w - 62)} \times 100\%$$

where M_w is the molecular weight of dye anion, 352.39 for AY36 and 377.39 for AR88.

The results show the MgAl-AR88-LDH shows a degree of intercalation of 97%, which means almost all the nitrate ions (NO_3^-) in the interlayer region have been exchanged for AR88 anions. MgAl-AY36-LDH has also achieved 88% successful substitution.

The TG and DTG curves obtained in a N_2 atmosphere are presented in Figure 7, revealing that the MgAl-NO_3-LDH and d-LDHs show very similar thermal decomposition behavior. That means the intercalation of AY36 and AR88 into the interlayer region of LDH did not decrease the thermal stability of LDH. Moreover, d-LDHs show better thermal stability than MgAl-NO_3-LDH below 600 °C. This can be attributed to the thermal stability of AY36 and AR88 anions, which restrained thermal decomposition of LDH to some degree, especially in the primary degradation stage.

Table 1. Thermogravimetric Analysis of d-LDHs

sample	T_5[a] (°C)	$T_{max}(1)$[b] (°C)	$T_{max}(2)$[b] (°C)	char yield at 800 °C (%)
MgAl-NO_3-LDH	170	371	468	59.7
MgAl-AY36-LDH	266	384	530	58.1
MgAl-AR88-LDH	209	335	504	56.0

[a]Temperature of the 5% weight loss. [b]Temperature of the maximal rate of weight loss under a nitrogen atmosphere.

3.2. Morphological Analysis of PP-g-MA/LDHs Composites. *3.2.1. WAXS.* The WAXS patterns of PP-g-MA/NO_3-LDH, PP-g-MA/SDBS-LDH, and PP-g-MA/d-LDH composites are shown in Figure 8. For the PP-g-MA/SDBS-LDH

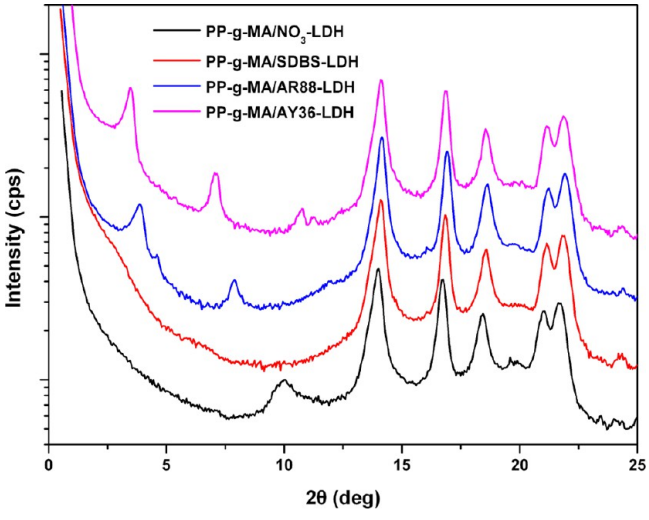

Figure 8. WAXS patterns of PP-g-MA/NO_3-LDH, PP-g-MA/SDBS-LDH, and PP-g-MA/d-LDH composites.

composite, the diffraction peak at $2\theta = 2.96°$ attributed to the first basal reflection (003) of SDBS-intercalated LDH disappeared, indicating that the SDBS-intercalated LDH might be exfoliated in the matrix. For PP-g-MA/NO_3-LDH and PP-g-MA/AR88-LDH composites, the diffraction peaks at $2\theta = 11.6°$ and 3.85° attributed to the first basal reflection (003) of NO_3^- and AR88-intercalated LDHs still exist,

dx.doi.org/10.1021/am4020555 | ACS Appl. Mater. Interfaces 2013, 5, 8991−8997

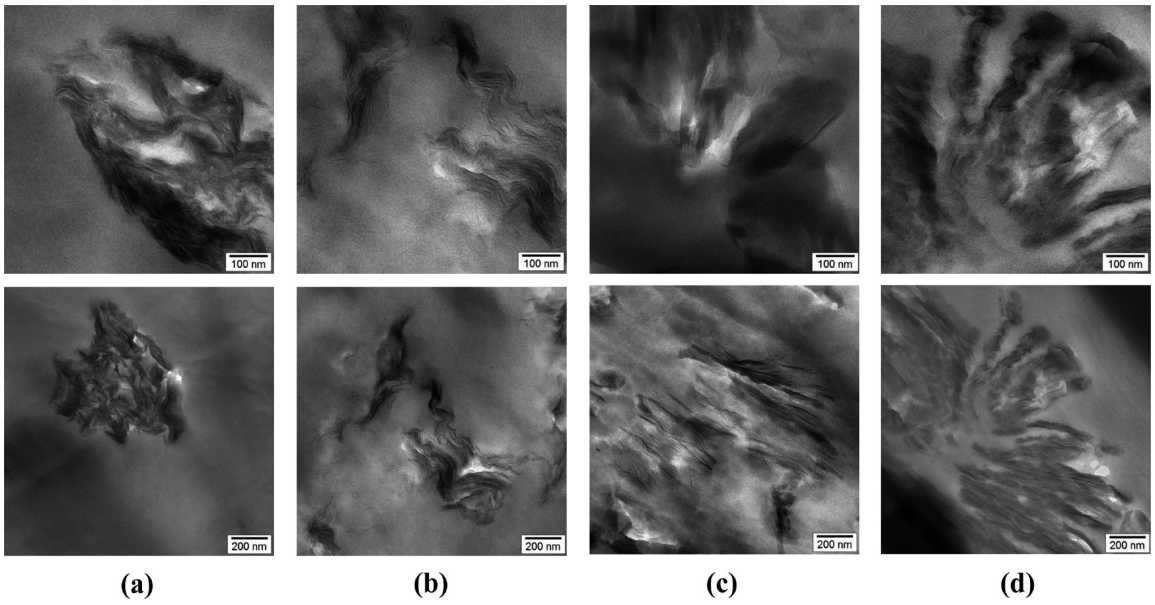

Figure 9. TEM images of PP-g-MA/LDH composites: (a) MgAl-NO_3-LDH, (b) MgAl-SDBS-LDH, (c) MgAl-AY36-LDH, and (d) MgAl-AR88-LDH.

indicating that the PP-g-MA polymer chains cannot totally penetrate into the gallery region of metal hydroxides. As with the PP-g-MA/AR88-LDH composite, there is an apparent peak at 2θ = 3.45° for the PP-g-MA/AY36-LDH composite. It means AY36-intercalated LDH is not exfoliated in the PP-g-MA matrix. However, in comparison to (006) and (009) basal reflections of AY36-LDH and AR88-LDH, PP-g-MA/AY36-LDH and PP-g-MA/AR88-LDH composites show weak and broad reflections. This may be attributed to a mixed morphology of unordered dispersion of LDHs in the matrix. The absence of full exfoliation of LDH in the polymer matrix is due to the strong affinity of the interlayer of d-LDH or the difference in the surface energy between AR88 and PP-g-MA and between AY36 and PP-g-MA.

3.2.2. TEM. TEM analysis gives direct information about the dispersion state of d-LDH particles in the polymer matrix. The morphology of composites was investigated by TEM and is shown in Figure 9. It is observed that the TEM micrographs of the PP-g-MA/d-LDHs are different from those of PP-g-MA/MgAl-NO_3-LDH. In the case of PP-g-MA/MgAl-NO_3-LDH, LDH aggregations are quite often observed in the polymer matrix and the average size of the aggregate is >500 nm. Compared to the dispersion state of PP-g-MA/MgAl-NO_3-LDH (Figure 9a), PP-g-MA/d-LDH shows relatively good dispersion of LDH in the matrix (Figure 9c,d), showing the smaller particle sizes (<200 nm). Although the aggregate sizes become small, the demoted aggregations in both PP-g-MA/AR88-LDH and PP-g-MA/AY36-LDH are still present. This is the reason why in the WAXS patterns of PP-g-MA/MgAl-NO_3-LDH and PP-g-MA/AR88-LDH the diffraction peaks are very similar with those of unmodified LDH and d-LDH. However, in fact, the dispersion states of LDH in the matrix between PP-g-MA/MgAl-NO_3-LDH and PP-g-MA/AR88-LDH are totally different. Among all the composites, PP-g-MA/SDBS-LDH provided the best LDH dispersion in the matrix. This is based on the WAXS results.

3.3. Thermal Stability of PP-g-MA/LDH Composites. Thermogravimetric analysis (TGA) is an effective technique for evaluating the thermal stability of the polymer. Figure 10

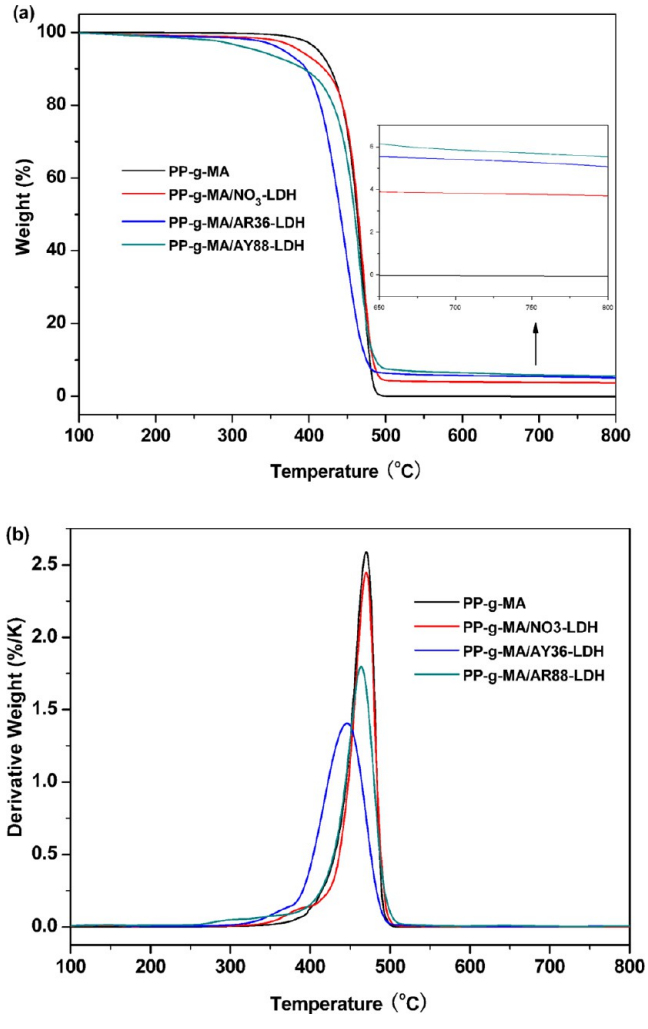

Figure 10. TGA profiles for PP-g-MA, PP-g-MA/NO_3-LDH, PP-g-MA/AR88-LDH, and PP-g-MA/AY36-LDH.

dx.doi.org/10.1021/am4020555 | ACS Appl. Mater. Interfaces 2013, 5, 8991−8997

illustrates the TGA curves of PP-g-MA and PP-g-MA/LDH composites. It is noted that an approximate 15% weight loss for PP-g-MA/AR88-LDH is in the range from 200 to 408 °C; a similar weight loss for PP-g-MA/AY36-LDH is in the range from 200 to 420 °C. This weight loss can be attributed to the thermal degradation of PP-g-MA and the decomposition of MgAl-LDH, meaning the d-LDH causes the earlier initial decomposition of composites in comparison to PP-g-MA. The maximal thermal decomposition temperature of PP-g-MA/d-LDH composites is also lower. However, as shown in Figure 10, the TGA curve of PP-g-MA shows no residue at 500 °C, whereas PP-g-MA/AR88-LDH and PP-g-MA/AY36-LDH composites have ~5.5 and ~5.1% residues, respectively, above 500 °C that persist until 800 °C. If we suppose there is no interaction upon formation of the char between LDH and PP-g-MA, on the basis of the char residue of each component (LDH and PP-g-MA), the char residues of PP-g-MA/AR88-LDH and PP-g-MA/AY36-LDH at 800 °C can be calculated (results listed in Table 2). Obviously, the calculated char residues of PP-g-MA/AR88-LDH and PP-g-MA/AY36-LDH are 2.9 and 2.8%, respectively, which are much lower than measured results (5.5 and 5.1%, respectively). These results indicate there are strong interactions upon formation of char residues between PP-g-MA and AR88-LDH/AY36-LDH, while these interactions between PP-g-MA and unmodified LDH are weak.

Table 2. Thermogravimetric Analysis of PP-g-MA and PP-g-MA/LDH Composites

sample	T_5[a] (°C)	T_{max}[b] (°C)	char yield at 800 °C (%, calculated)	char yield at 800 °C (%, measured)
PP-g-MA	412	470	–	–
PP-g-MA/MgAl-NO_3-LDH	388	470	3.0	3.7
PP-g-MA/AR88-LDH	333	464	2.9	5.5
PP-g-MA/AY36-LDH	367	446	2.8	5.1

[a]Temperature of the 5% weight loss. [b]Temperature of the maximal rate of weight loss under a nitrogen atmosphere.

3.4. Flame Retardancy of PP-g-MA/LDH Composites. Figure 11 shows the HRR plots for d-LDH, PP-g-MA, PP-g-MA/NO_3-LDH, PP-g-MA/SDBS-LDH, and PP-g-MA/d-LDH measured by microscale combustion calorimetry (MCC), and the corresponding combustion data are listed in Table 2. In Figure 10a, it can be seen that HRR values of MgAl-AR88-LDH and MgAl-AY36-LDH are similar and PP-g-MA has a high HRR value (1014 W/g). According to each individual component and the relative proportion, the calculated values of HRR and HRC for PP-g-MA/d-LDH can be obtained if there is no interacting influence of the pyrolysis process of the material. It is clear that the pHRR value decreases significantly upon addition of d-LDHs. In detail, the pHRR of PP-g-MA is 1043 W/g; it decreases to 927 W/g in PP-g-MA/SDBS-LDH, 812 W/g in PP-g-MA/AR88-LDH, and 702 W/g in PP-g-MA/AY36-LDH, indicating flame resistance is improved significantly. In comparison to the calculated values of HRR listed in Table 2, it is easy to find that the measured HRR values of PP-g-MA/d-LDH composites are much lower. In addition, in comparison to the HRRs of PP-g-MA/NO_3-LDH and PP-g-MA/SDBS-LDH composites, HRRs of PP-g-MA/d-LDH composites are also much lower. The decrease in the flammability of PP-g-MA/d-LDH is most likely from the charring effect of the sulfuric acid generated from the thermal decomposition of the sulfate dyes, which is ascribed to the TGA results.

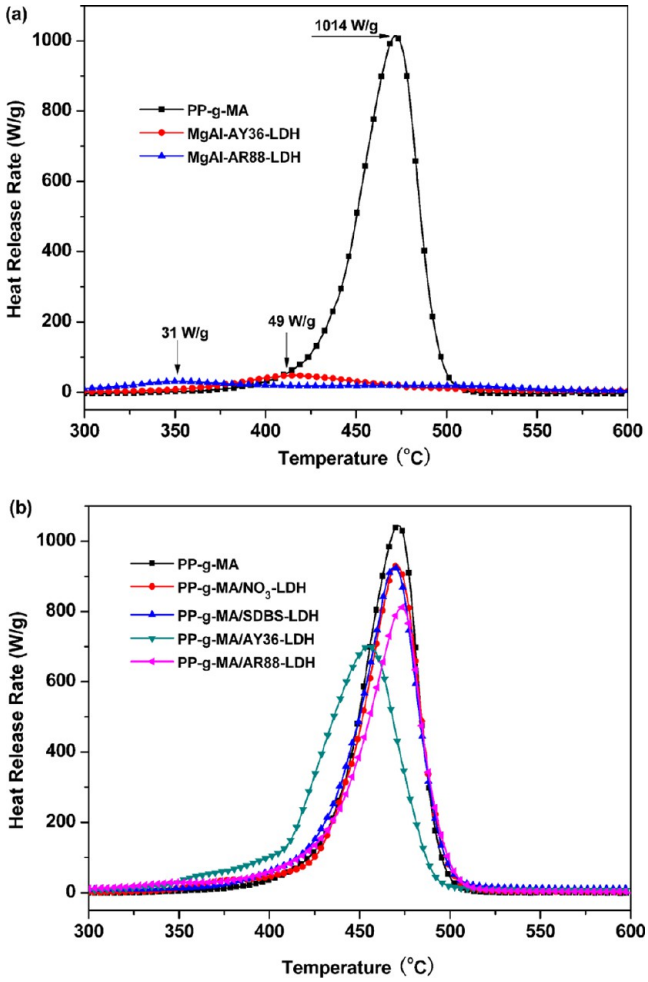

Figure 11. HRR curves of (a) d-LDHs and (b) PP-g-MA/LDH composites at a heating rate of 1 K/s.

The total heat release (THR) is also an important parameter for evaluating the flame retardancy of a material. It can be clearly seen in Table 3 that THR values of PP-g-MA, PP-g-MA/AR88-LDH, and PP-g-MA/AY36-LDH composites are 40.3, 33.2, and 38.0 kJ/g, respectively, showing that the addition of d-LDH leads to an improvement in the flame retardancy of the composites. The trend is similar to that of the HRR. Additionally, the temperature at the maximal pyrolysis rate

Table 3. Data Recorded in MCC Measurements

sample	pHRR-c[a] (W/g)	pHRR-m[b] (W/g)	THR (kJ/g)	T_{max} (°C)
MgAl-AR88-LDH	–	31 ± 1	–	350
MgAl-AY36-LDH	–	49 ± 1	–	417
PP-g-MA	–	1043 ± 20	40.3 ± 0.6	471
PP-g-MA/NO_3-LDH	–	930 ± 30	38.0 ± 1.5	470
PP-g-MA/SDBS-LDH	–	927 ± 35	38.6 ± 1.8	469
PP-g-MA/AR88-LDH	992	812 ± 15	33.2 ± 1.9	474
PP-g-MA/AY36-LDH	993	702 ± 38	38.0 ± 0.8	455

[a]Calculated peak heat release rate. [b]Measured peak heat release rate.

(T_{max}) shows no significant difference between the composites and the neat polymer.

4. CONCLUSION

In this paper, dye-intercalated LDHs (d-LDH) have been synthesized via a one-step method and used to improve the flame retardancy of PP-g-MA/d-LDH composites, which were prepared by refluxing 5 wt % d-LDH and 95 wt % PP-g-MA in xylene. The intercalated behaviors of d-LDH were characterized by FTIR, WAXS, SEM, TGA, and elemental analysis. The WAXS results revealed the d-LDHs possess a >3-fold increase in interlayer distance compared to that of MgAl-NO_3-LDH. The elemental analysis results confirmed MgAl-AR88-LDH and MgAl-AY36-LDH show degrees of intercalation of 97 and 88%, respectively. The WAXS and TEM results for PP-g-MA/d-LDHs composites illustrated the formation of a mixed morphology of unordered dispersion of LDHs in the matrix. The combustion behaviors of PP-g-MA and PP-g-MA/d-LDH composites were investigated with a microscale combustion calorimeter, which revealed that incorporation of d-LDHs was very efficient in reducing the flammability of PP-g-MA composites. In detail, the pHRR and THR of PP-g-MA are 1043 W/g and 40.3 kJ/g, respectively. In comparison, they decreased to 812 W/g and 33.2 kJ/g, respectively, in PP-g-MA/AR88-LDH and 702 W/g and 38.0 kJ/g, respectively, in PP-g-MA/AY36-LDH. These results indicate the introduction of small amounts of d-LDH significantly reduces the flammability of PP-g-MA, offering a new approach to imparting low flammability to LDH-based polymer composites.

AUTHOR INFORMATION

Corresponding Author

*E-mail: deyi.wang@imdea.org.

Notes

The authors declare no competing financial interest.

ACKNOWLEDGMENTS

This research is partly funded by the European Commission under the 7th Framework Programme (Marie Curie Career Integration Grant) and European Project COST Action MP1105 "FLARETEX".

REFERENCES

(1) Wang, D. Y.; Leuteritz, A.; Kutlu, B.; Landwehr, M. A.; Jehnichen, D.; Wagenknecht, U.; Heinrich, G. *J. Alloys Compd.* **2011**, *509*, 3497−3501.
(2) Costa, F. R.; Wagenknecht, U.; Heinrich, G. *Polym. Degrad. Stab.* **2007**, *92*, 1813−1823.
(3) Aisawa, S.; Kudo, H.; Hoshi, T.; Takahashi, S.; Hirahara, H.; Umetsu, Y.; Narita, E. *J. Solid State Chem.* **2004**, *177*, 3987−3994.
(4) Hibino, T. *Chem. Mater.* **2004**, *16*, 5482−5488.
(5) Whilton, N. T.; Vickers, P. J.; Mann, S. *J. Mater. Chem.* **1997**, *7*, 1623−1629.
(6) Wilson, O. C.; Olorunyolemi, T.; Jaworski, A.; Borum, L.; Young, D.; Siriwat, A.; Dickens, E.; Oriakhi, C.; Lerner, M. *Appl. Clay Sci.* **1999**, *15*, 265−279.
(7) Leroux, F.; Besse, J. P. *Chem. Mater.* **2001**, *13*, 3507−3515.
(8) Zhao, C. X.; Liu, Y.; Wang, D. Y.; Wang, D. L.; Wang, Y. Z. *Polym. Degrad. Stab.* **2008**, *93*, 1323−1331.
(9) Wang, D. Y.; Leuteritz, A.; Wang, Y. Z.; Wagenknecht, U.; Heinrich, G. *Polym. Degrad. Stab.* **2010**, *95*, 2474−2480.
(10) Wang, D. Y.; Das, A.; Costa, F. R.; Leuteritz, A.; Wang, Y. Z.; Wagenknecht, U.; Heinrich, G. *Langmuir* **2010**, *26*, 14162−14169.
(11) Chen, W.; Qu, B. *Chem. Mater.* **2003**, *15*, 3208−3213.
(12) Darder, M.; Mar, L. B.; Aranda, P.; Leroux, F.; Eduardo, R. H. *Chem. Mater.* **2005**, *17*, 1969−1977.
(13) Illaika, A.; Vuillermoz, C.; Commereuc, S.; Taviot-Gueho, C.; Verney, V.; Leroux, F. *J. Phys. Chem. Solids* **2008**, *69*, 1362−1366.
(14) Wang, D. Y.; Wang, Y. Z.; Wang, J. S.; Chen, D. Q.; Zhou, Q.; Yang, B.; Li, W. Y. *Polym. Degrad. Stab.* **2005**, *87*, 171−176.
(15) Shabanian, M.; Kang, N. J.; Wang, D. Y.; Wagenknecht, U.; Heinrich, G. *Polym. Degrad. Stab.* **2013**, *98* (5), 1036−1042.
(16) Wang, D. Y.; Das, A.; Leuteritz, A.; Mahaling, R. N.; Jehnichen, D.; Wagenknecht, U.; Heinrich, G. *RSC Adv.* **2012**, *2*, 3927−3933.
(17) Pereira, C. M. C.; Herrero, M.; Labajos, F. M.; Marques, A. T.; Rives, V. *Polym. Degrad. Stab.* **2009**, *94*, 939−946.
(18) Nyambo, C.; Kandare, E.; Wilkie, C. A. *Polym. Degrad. Stab.* **2009**, *94*, 513−520.
(19) Rives, V.; Ulibarri, M. A. *Coord. Chem. Rev.* **1999**, *181*, 61−120.
(20) Qiu, L.; Chen, W.; Qu, B. *Polym. Degrad. Stab.* **2005**, *87*, 433−440.
(21) Liao, C. S.; Ye, W. B. *J. Polym. Res.* **2003**, *10*, 241−246.
(22) Ding, P.; Qu, B. *Polym. Eng. Sci.* **2006**, *46*, 1153−1159.
(23) Nhlapo, N.; Motumi, T.; Landman, E.; Verryn, S. M. C.; Focke, W. W. *J. Mater. Sci.* **2008**, *43*, 1033−1043.
(24) Iyi, N.; Ebina, Y.; Sasaki, T. *J. Mater. Chem.* **2011**, *21*, 8085−8095.
(25) Moujahid, E. M.; Besse, J. P.; Leroux, F. *J. Mater. Chem.* **2003**, *13*, 258−264.
(26) Woo, M. A.; Kim, T. W.; Paek, M. J.; Ha, H. W.; Choy, J. H.; Hwang, S. J. *J. Solid State Chem.* **2011**, *184*, 171−176.
(27) Choy, J. H.; Kwak, S. Y.; Park, J. S.; Jeong, Y. J.; Portier, J. *J. Am. Chem. Soc.* **1999**, *121*, 1399−1400.
(28) Costa, F. R.; Goad, M. A.; Wagenknecht, U.; Heinrich, H. *Polymer* **2005**, *46*, 4447−4453.
(29) Wang, D. Y.; Costa, F. R.; Vyalikh, A.; Leuteritz, A.; Scheler, U.; Jehnichen, D.; Wagenknecht, U.; Haussler, L.; Heinrich, G. *Chem. Mater.* **2009**, *21*, 4490−4497.
(30) Vyalikh, A.; Wang, D. Y.; Wagenknecht, U.; Heinrich, H.; Scheler, U. *Chem. Phys. Lett.* **2011**, *509*, 138−142.
(31) Gu, L.; Zhu, N.; Wang, L.; Bing, X.; Chen, X. *J. Hazard. Mater.* **2011**, *198*, 232−240.
(32) Hihara, T.; Okada, Y.; Morita, Z. *Dyes Pigm.* **2007**, *75*, 585−605.